Universidad Zaragoza
1542

Trabajo Fin de Máster

Systematic study on the biomechanical stability of C-loop intraocular lenses:
Approach to an optimal design of the haptics

Estudio sistemático de la estabilidad biomecánica de lentes intraoculares C-loop:
Enfoque a un diseño óptimo de los hápticos

Autor

Iulen Cabeza Gil

Directora

Begoña Calvo Calzada

Codirector

Miguel Ángel Ariza Gracia

EINA, Universidad de Zaragoza

2019

Agradecimientos

Sirvan estas líneas para agradecer a varias personas por haber contribuido a terminar este Trabajo Fin de Máster.

Agradecer a mi directora la oportunidad de trabajar en este proyecto. Cuando el esfuerzo se convierte en un hobby y en una costumbre, el éxito se convierte en una constante, Gracias Begoña.

Trabajar con Miguel Ángel me ofrece oportunidades impensables para seguir progresando y desarrollándome como investigador, Gracias MA.

Agradecer a Laura Remón su dedicación y esfuerzo, sin ella este trabajo no hubiera sido posible. Gracias Laura por tus consejos.

Agradecer a Jesus Pérez la confianza y el apoyo en este trabajo, fabricando las lentes óptimas para ensayarlas experimentalmente. Espero que sigamos colaborando en nuestra tesis juntos.

Agradecer a mis compañeros de la sala por sus consejos en la elaboración del trabajo.

Por último, agradecer a las personas que desde que nací han sido mis dos pilares, haciendo posible que pueda meter tantas horas a lo que verdaderamente me inquieta. Gracias padres.

Resumen

El objetivo de este Trabajo Fin de Máster es estudiar la influencia de los parámetros que definen la geometría de las lentes intraoculares C-loop que afectan a la estabilidad mecánica en el saco capsular. Dando lugar a un diseño óptimo de lente C-loop que minimiza el desplazamiento axial, la inclinación y la rotación.

Se estudiaron un total de 144 variaciones geométricas de una lente intraocular C-loop no angulada. El conjunto de variaciones adecuado se determinó mediante un análisis factorial mixto, que permitió analizar el impacto de los diferentes diseños sobre la estabilidad mecánica de la lente (fuerza de compresión, desplazamiento axial, inclinación y rotación). Los parámetros de diseño estudiados fueron: la longitud, anchura, espesor y ángulo de apertura del háptico, la unión háptico-óptica y el inicio de la curvatura háptica. El impacto de los diferentes parámetros se evaluó mediante gráficos de Pareto y análisis estadísticos.

La fuerza de compresión (o reacción) se ve afectada por la anchura del háptico, la unión háptico-óptica y la interacción entre ambas. El desplazamiento axial se ve afectado principalmente por la anchura y el grosor del háptico, así como por el tamaño de la unión háptico-óptica. La inclinación se ve afectada por el espesor háptico y la interacción entre la curvatura háptica y la unión háptico-óptica. La rotación se ve afectada por el inicio de la curvatura háptica, la unión háptico-óptica y la anchura del háptico.

La principal conclusión de este TFM es que la unión háptico-óptica es uno de los parámetros más influyentes que afectan en las cuatro respuestas estudiadas de las lentes C-Loop. Cuanto más pequeña sea la unión háptico-óptica, mejor será la estabilidad biomecánica.

Abstract

To study the main design parameters that affect the mechanical stability of C-loop intraocular lenses, leading to an optimal design that minimizes the axial displacement, tilt and rotation.

A total of 144 geometrical variations were studied on a 1-piece, non-angulated, C-loop hydrophobic intraocular lens. The suitable set of variations was determined using a mixed-factorial analysis, allowing to analyse the impact of the different designs on the mechanical stability of the lens (compression force, axial displacement, tilt and rotation). The design parameters under study were: the length, width, thickness and opening angle of the haptic, the haptic-optic junction and the start of the haptic curvature. The impact of the different parameters was evaluated using Pareto charts and statistical analysis.

The compression (or reaction) force is affected by the haptic width, the haptic-optic junction, and the interaction between both. The axial displacement is mainly affected by the width and thickness of the haptic, and the size of the haptic-optic junction as well. The tilt is affected by the haptic thickness and the interaction between the haptic curvature and the haptic-optic junction. The rotation is affected by the start of the haptic curvature, the haptic-optic junction, and the haptic width.

The main conclusion of this TFM was that the haptic-optic juntion is one of the most influential parameters affecting the four responses studied of the C-Loop IOL. The smaller the haptic-optic juntion, the better biomechanical stability.

Contents

Chapter 1

Introduction

The most widely performed surgery in ophthalmology is cataract surgery, see Fig.1.1. Nowadays this intervention increasingly seeks not only to substitute the opaque lens by an intraocular lens, but also to achieve emmetropia, the independence of the glasses, either at a distance, with monofocal lenses, or at various distances, with multifocal lenses.

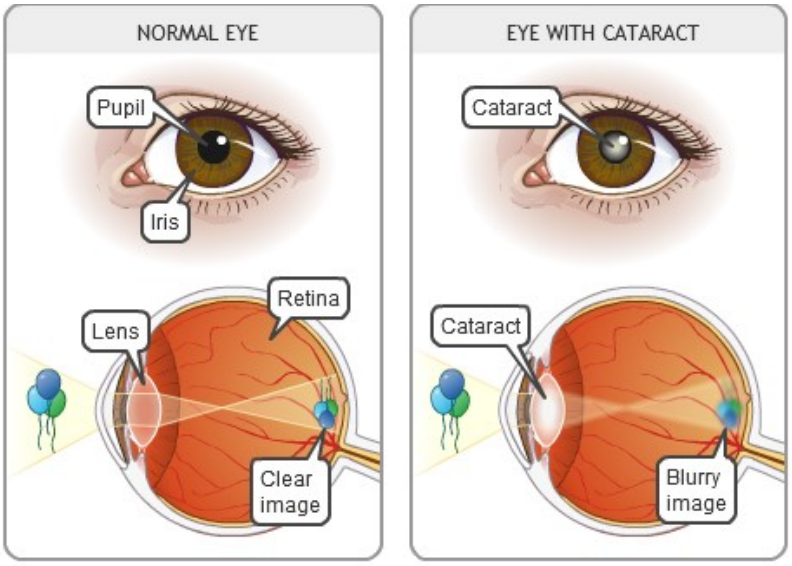

Figure 1.1: Comparative between a normal/healthy and a eye with cataract. Cataracts occur when the lens of the eye, which is normally clear, becomes cloudy or opaque. Light that passes through the lens becomes scattered and diffuse, leading to blurred vision, light sensitivity, and more trouble differentiating colors and seeing in low contrast situations. *Recovered from https://www.aboutkidshealth.ca.*

The biomechanical stability of the IOL inside the capsular bag is essential to ensure a successful surgical procedure. Rotation is a crucial factor in toric[1] and asymmetrical multifocal[2] IOLs, while decentration and tilt are important in pupil-dependent multifocal and aspheric IOLs.[3,4] These parameters affect the optical performance and efficacy of these IOLs, resulting in significant visual disturbances,[5] see Fig.1.2.

Rotation, decentration or tilt mainly occur in the early postoperative period, right before fusing the anterior and posterior capsule with the IOL.[6] Material properties,[7] haptic design[8,9] and size[10] of the IOL are considered to be very influential factors in the postoperative IOL stability. Incomplete viscoelastic clearance, early postoperative IOL fluctuations, capsulorhexis size and axial length are other influencing factors.[11,12]

After the first poly-methyl-methacrylate (PMMA) IOL was implanted by Harold Ridley in 1949,[13] hydrophobic acrylic, hydrophilic acrylic, and silicone[14] foldable materials have been developed to allow removing the cataract through smaller incisions. Morever, a variety of IOLs with different optic size,[11,15] edge profiles,[16] haptic materials and designs[8,9,17] have been developed to minimize decentration, dislocations and tilt. But industry has emphasized the design of the haptics, leading to different revolutionary designs such as plate, plate-loop or open-loop (C-loop, J-loop and Double-C loop) style with planar and angulated haptics.[18–22]

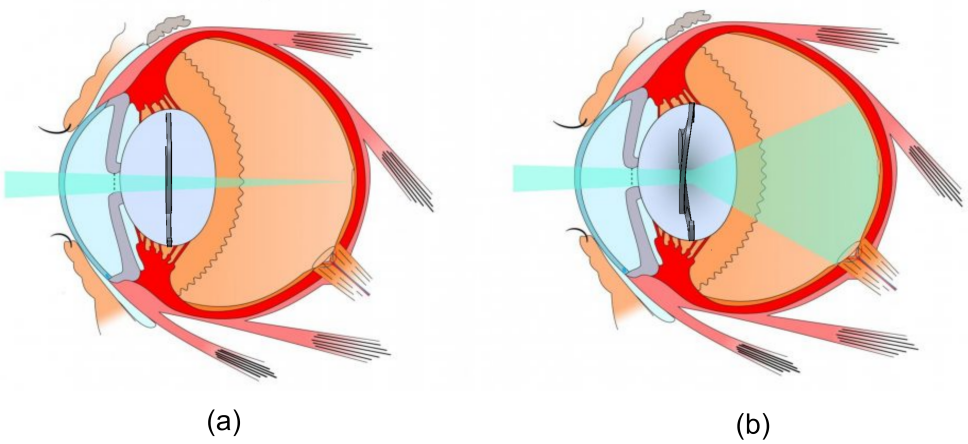

Figure 1.2: Cross section view of a eyeball with a IOL. (a) Adequate position of the IOL. (b) Bad positioning of the IOL. *Edited from an image of https://www.shutterstock.com/.*

Within this plethora of designs, see Fig.1.3, C-loop haptics have been suggested to ensure a better stabilization and centration than IOLs with plate-like haptics,[19,20,23] except for silicone-made haptics, for which plate haptics showed better rotational stability.[21] In terms of axial stability, planar haptic designs perform better than angulated designs, reducing the impact in the final refractive errors.[24–27] Finally, single-piece IOLs exhibited better axial stability and more stable refractive outcomes than three-pieces IOLs, presenting no difference in decentration or optic tilt.[17,28]

Another important factor that has been suggested to determine the biomechanical stability of the IOL is the size of the lens. For larger capsular bags, IOLs with smaller diameters had a higher risk of presenting axial displacement, decentration or tilt. Furthermore, IOLs rotated more in eyes with longer axial lengths, which often have a bigger capsular bag diameter than highly hyperopic eyes.[11,15] Despite the existence of a plethora of designs, all IOLs are manufactured with a total fixed diameter, neglecting either the inherent patient's variability of the capsular bag, which ranges from 9.6 mm to 10.2 mm, or the axial length of the eyeball.

Although there are several methods to measure decentration, tilt or rotation after implantation in a pseudophakic eye,[29,30] IOLs must have strict performance features to reliably predict their mechanical behavior. The International Organization for Standardization specifies guidelines and testing methods for certain biomechanical properties of IOLs (ISO 11979-3).[31]

Biomechanical stability of different commercial IOLs with different materials has been studied experimentally[19,27,32] and numerically.[25] In a previous study, we used finite element modelling (FEM) to evaluate the biomechanical stability of four different hydrophobic and hydrophilic IOLs with different haptic designs following the procedure described in the ISO 11979-3.[25] In particular, the material and the

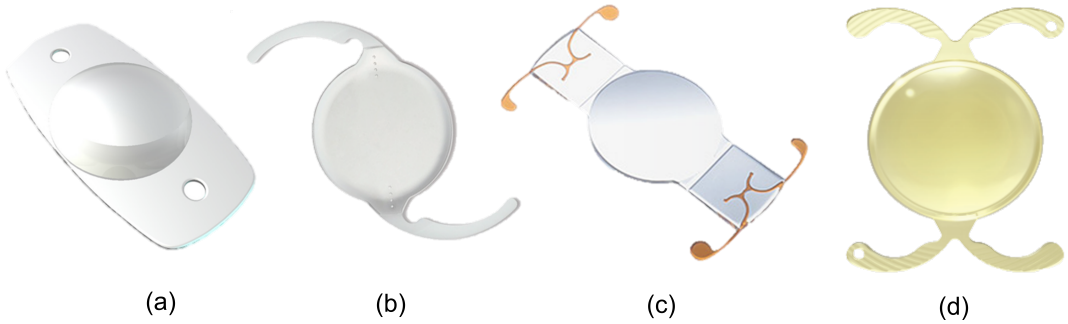

Figure 1.3: Several design of intraocular lenses. (a) Plate design. (b) C-loop design. (c) Plate-loop design. (d) Double-C loop design. *Edited from several images.*

design were found to be of importance on the postoperative behavior of an IOL.

This work presents the first systematic study based on Design of Experiments and in silico modelling to evaluate the effect of key design parameters on the mechanical stability of a 1-piece hydrophobic IOL with non-angulated C-loop haptics. The C-loop design was chosen as benchmark since it presents better stability and centration than other multipiece, angulated or plate designs.[22] Likewise, an hydrophobic material was used as it presents a higher level of adhesiveness than hydrophilic or silicone, being a gold standard to prevent the posterior capsule opacification.[33] Geometric design parameters studied were: the length, width, thickness and opening angle of the haptic, the haptic curvature start, and the haptic-optic junction. In silico analysis was performed using a finite element (FE) model, simulating the dynamic compression procedure described in the Standard ISO 11979-3.[31] A dataset of 216 geometrical variations was analysed to determine the lens that guarantees the best biomechanical stability (i.e., axial displacement, tilt, and rotation). The presented methodology can help manufacturers during the design phase, clinicians to know which IOLs present better stability based on the design, and represents a first step towards the customization of IOLs.

1.1 Motivation

According to the World Health Organization, in 2010, 285 million people were visually impaired and 39 million were blind. The two main causes of visual impairment in the world are uncorrected refractive errors (42%) and cataracts (33%). 82% of blind people and 65% with moderate blindness were over the age of 50.[34]

The only current treatment for cataracts is by implanting an IOL that replaces the opacified crystalline lens. The implantation of an IOL is an invasive procedure (Fig.1.4) and it meets thus minimum requirements to ensure good optical quality and provide good stability within the capsule bag in the final postoperative outcome.

In this work, several simulations will be carried out to find an optimal design for C-loop IOLs according to ISO 11979-3:2013.[31] This standard describes tests that evaluate the mechanical properties of IOLs to ensure good IOL stability within the capsule bag.

The results obtained in this Master's Thesis will be very useful in the design phase as it will save time and costs due to the reduction of intermediate prototypes manufactured to reach the optimal design. AJL Ophtalmic S.A., (http://ajlsa.com), participates in this work providing us with the material under study, acrylic hydrophobic (BENZ HF 1.2)[35] and it is interested in our results in order to modify future IOL designs.

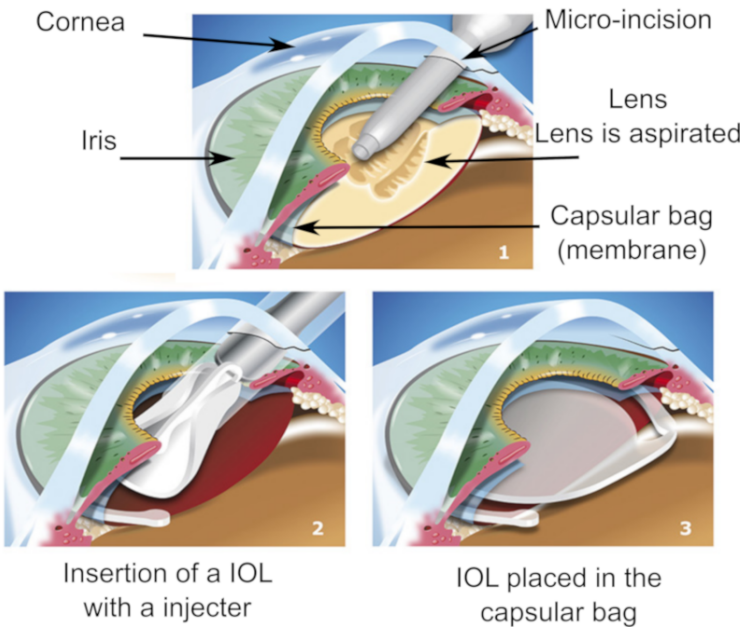

Figure 1.4: Emplacement of an intraocular lens in the eyeball. *Edited from an image of https://www.corneaconsultants.com/cataracts/.*

1.2 Objetive

The overall objective of this Master's Thesis (TFM) is to find an optimal design of C-loop intraocular lens. In order to guarantee this global objective, the following specific objectives have been established:

- Reproduce $in-silico$ the main mechanical compression tests established in ISO 11979-3[31] in order to improve their design stage.
- Experimentally characterize the mechanical response of the material commonly used in the manufacture of IOLs, hydrophobic acrylic plastic.
- Determine the geometry of the haptics using the minimum number of parameters.
- Propose a numerical model of material behavior that correctly fits the experimental results.
- Statistical analysis of the results obtained, that is to say, analyse the effect of each parameter on the biomechanical stability of the IOL.

1.3 Content

The TFM has been organized into 4 chapters which are described below:

- **Introduction.** The purpose of this chapter is to focus and attract the reader towards cataract surgery and the study of intraocular lenses, defining the different typologies, as well as establishing the objectives of the TFM and its contents.
- **Material and Methods.** This chapter describes the mechanical compression tests developed to characterize the hydrophobic acrylic material under study, as well as its characterization by means of a hyperelastic model. Subsequently, The design of experiments performed is described, including the design parameters under study. Finally, the finite element model for calculating the simulation is exposed.
- **Results.** This chapter describes the results obtained in the experiment. The influence of each parameter on the different responses studied (reaction-compression force, axial displacement, tilt, and rotation) is shown.
- **Conclusion and Future Lines.** Finally, the results obtained will be discussed, the main conclusions of this study will be summarised, and possible future lines from this project will be referenced.

Chapter 2

Materials & Method

This chapter describes the mechanical compression and tensile/tension tests developed to characterize the material under study, hydrophobic acrylic (Benz HF-1.2 Natural Yellow) provided by the company AJL Ophtalmic S.A. Consequently, a hyperelastic numerical model that reproduces the experimental data collected is proposed. Then, the experimental design methodology used to analyse the biomechanical design of intraocular lenses is described. Finally, the method used to numerically simulate the ISO 11979-3[31] compression test is explained.

2.1 Mechanical characterization of hydrophobic acrylic material

The behaviour of the material was analysed using two types of test pieces as showed in Fig.2.1, in accordance with the ISO standards for compression and tensile strength.[36,37] The mechanical response was studied as a function of temperature (20 and 35 *degrees Celsius*) and considering the material dry or immersed in a physiological solution for 72 *hours*. Three test pieces were analysed for each type of variable, temperature and humidity. Each test piece was undergone 72 h conditioning. The test pieces were weighed before and after conditioning. The submerged test pieces increased their weight between 1.6 % and 2.3 % of their initial weight.

The uniaxial compression tests were performed at a speed of 1 $mm/minute$ under displacement control on an INSTRON 5548 machine, using a 150 N full scale load cell. The preparation of the machine was carried out before starting the tests. The test parameters were introduced into the software that manages the machine, indicating the sample dimensions and test conditions: number of preconditioning cycles and maximum deformation level in these cycles, machine speed in the test

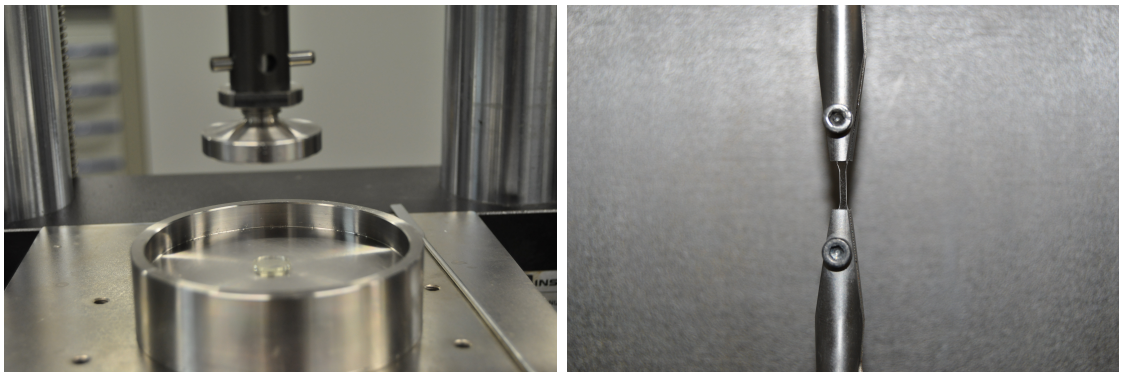

(a) (b)

Figure 2.1: Test pieces used on a INSTRON 5548 machine: a) Compression test piece. The compression test pieces had a dimension of 13.15 mm of diameter and a thickness of 2.17 mm. b) Tensile/Tension test piece. The tensile test pieces had a length of 8 mm, a thickness of 0.8 mm and an initial width of 1.10 mm.

and completion conditions. Samples were subjected to four loading/unloading cycles up to 20 % deformation in compression and until its breaking point in tensile. With the data recorded during the test, the deformation was calculated as $\lambda = \frac{\Delta L}{L_0}$, where L_0 was the initial distance between clamps and ΔL was the displacement of the upper clamp. The nominal tension or first tensioner of Piola-Kirchhoff was obtained as $P = \frac{N}{A_0}$, where N was the load recorded by the machine and A_0 was the initial area of the cross section of the test piece. The test pieces used for the compression tests were previously lubricated, but the material continued to adhere to the clamps. The tests performed were:

- 3 test pieces at 20 ^{o}C without being submerged (WS).
- 3 test pieces at 35 ^{o}C without being submerged (WS).
- 3 test pieces at 20 ^{o}C submergend during 72 h (S).
- 3 test pieces at 35 ^{o}C submergend during 72 h (S).

The wearing resistance of the material only for the compression test was also studied. *In total, 24 compression tests were carried out, plus 12 tensile tests, 36 tests.* For this purpose, the compression tests were repeated after 24 *hours* on the previously test pieces rehearsed. Nevertheless, the results were practically the same, in other words, there was no damage to the material.

2.1.1 Material curves for the 4 conditions tested

The results obtained after conducting the test are depicted in Fig.2.2. The blue line plots the compression curve of the material while the orange line plots the tensile/tension curve. The numerical tests were performed with the result at 35 ^{o}C (body temperature of the human body) and submerged in water, since it gathers similar conditions of the IOL in the capsular bag.

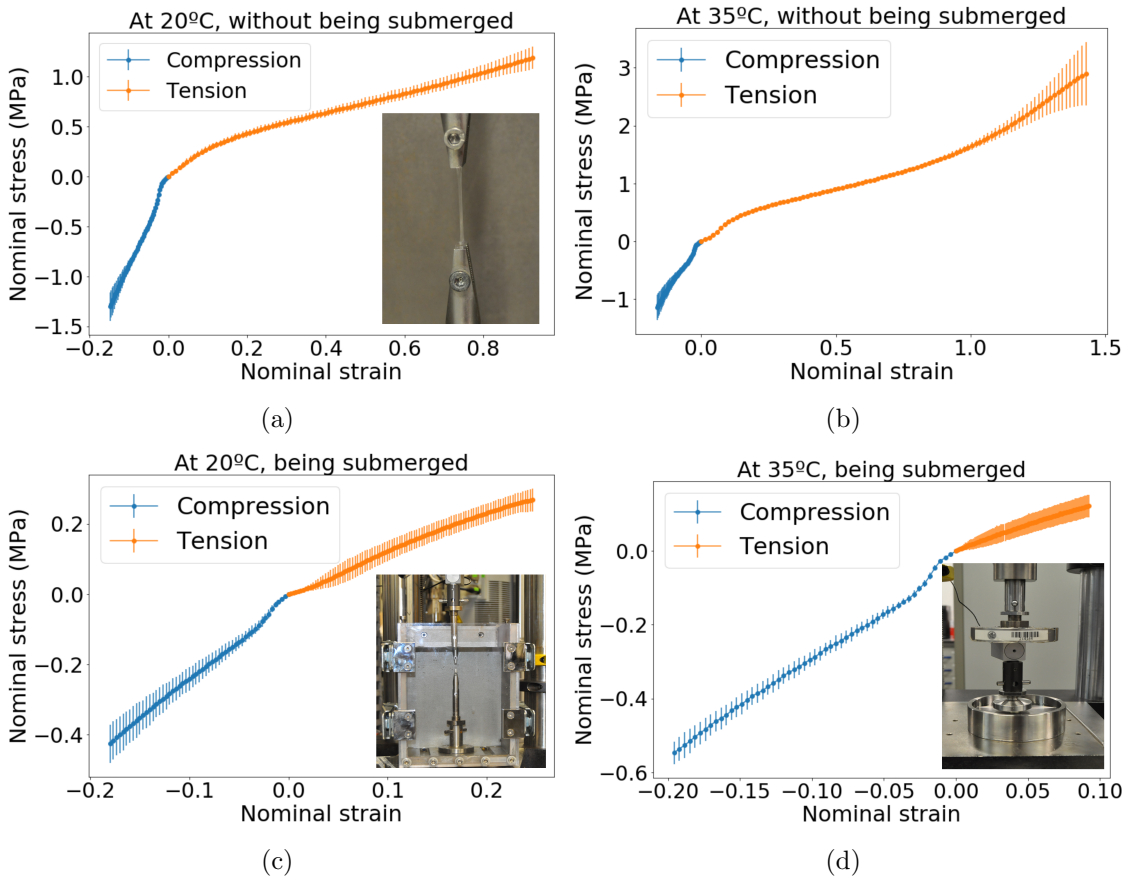

Figure 2.2: Comparative between tensile (blue) and compression (orange) curves for different conditionings: a) Hydrophobic material curve at 20 ^{o}C withouth being sumerged (WS). b) Hydrophobic material curve at 35 ^{o}C (WS). c) Hydrophobic material curve at 20 ^{o}C being sumerged (S). d) Hydrophobic material curve at 35 ^{o}C (S). The mean and deviation of the 3 tests tested are plotted.

The main conclusions of the material under study were:

- The material behaved differently to tensile and compression. Tensile was less rigid.
- As the humidity of the material increased, the material became more flexible.
- The hydrophobic material absorbed between 1.6 % and 2.3 % water from its total weight for a 72 h conditioning.
- There was no material damage in compression at 20 % levels of deformation in either dry or wet material.
- The tensile rupture of the wet material occurred at about 20 % of the deformation.
- The ultimate tensile strength of dry material occurred around 200 % of deformation.
- There were no significant differences in the behavior for the analysed temperatures.

2.1.2 Hyperelastic behavior model

After analysing the stress strain curve obtained in the compression test, a phenomenological behaviour model which describes the experimental response at a macroscopic level was necessary, i.e., a model able to reproduce the non-linear response with large deformations. In this TFM we focused on reproducing the elastic response of the material. Therefore, an isotropic hyperelastic model was selected, i.e., establishing a function of deformation energy density through exponential, polynomial or logarithmic functions. The representation of the decoupled strain energy density function Ψ was:[38]

$$\Psi = \Psi_{vol}(J) + \bar{\Psi}(\bar{\mathbf{C}}) = \Psi_{vol}(J) + \bar{\Psi}(\bar{I}_1, \bar{I}_2) \tag{2.1}$$

with Ψ_{vol} y $\bar{\Psi}$ the volumetric part and the deviator of the strain energy density function, respectively, and

$$\bar{I}_1 = \bar{\mathbf{C}}, \quad \bar{I}_2 = \frac{1}{2}((tr\bar{\mathbf{C}})^2 - tr\bar{\mathbf{C}}^2) \tag{2.2}$$

$\bar{I}_1$ y $\bar{I}_2$ are the first and $\bar{\mathbf{C}} = \bar{\mathbf{F}}^T\bar{\mathbf{F}}$ the second invariant of the right Cauchy-Green tensor.

The stress response was obtained from the strain energy density function taking into account the inequality of Clausius-Planck

$$\mathcal{D}_{int} = -\dot{\Psi} + \frac{1}{2}\mathbf{S} : \dot{\mathbf{C}} \geq 0 \tag{2.3}$$

through

$$\mathbf{S} = 2\frac{\partial \Psi}{\partial \mathbf{C}} = \mathbf{S}_{vol} + \bar{\mathbf{S}}_{iso} = Jp\mathbf{C}^{-1} + J^{-\frac{2}{3}}(\mathbf{I} - 1/3\mathbf{C}^{-1} \otimes \mathbf{C}) : \bar{\mathbf{S}} = Jp\mathbf{C}^{-1} + J^{-\frac{2}{3}}DEV[\bar{\mathbf{S}}] \tag{2.4}$$

where p is the hydrostatic pressure, DEV is the deviating operator in material description and, $\bar{\mathbf{S}}$ the second Piola-Kirchhoff stress tensor modified[39]

$$p = \frac{d\Psi_{vol}(J)}{dJ} \qquad\qquad \bar{\mathbf{S}} = 2\frac{\partial \bar{\Psi}(\bar{\mathbf{C}})}{\partial \bar{\mathbf{C}}} \tag{2.5}$$

The value of the second tensor of Piola-Kirchhoff as a function of the invariants $\bar{I}_1$, $\bar{I}_2$ was given by

$$\mathbf{S} = Jp\mathbf{C}^{-1} + 2[(\frac{\partial \bar{\Psi}}{\partial \bar{I}_1} + \bar{I}_1\frac{\partial \bar{\Psi}}{\partial \bar{I}_2})\mathbf{1} - \frac{\partial \bar{\Psi}}{\partial \bar{I}_2}\mathbf{C} - \frac{1}{3}(\frac{\partial \bar{\Psi}}{\partial \bar{I}_1}\bar{I}_1 + 2\frac{\partial \bar{\Psi}}{\partial \bar{I}_2}\bar{I}_2)\mathbf{C}^{-1}] \tag{2.6}$$

The Cauchy stress tensor σ was $1/J$ times the push (*push-forward*) of $\mathbf{S}$ ($\sigma = J^{-1}\chi_*(S)$), or in index notation, $\sigma_{ij} = J^{-1}F_{iI}F_{jJ}S_{IJ}$. Operating, it is obtained:

$$\sigma = p\mathbf{1} + \frac{2}{J}[(\frac{\partial \bar{\Psi}}{\partial \bar{I}_1} + \bar{I}_1\frac{\partial \bar{\Psi}}{\partial \bar{I}_2})\mathbf{b} - \frac{\partial \bar{\Psi}}{\partial \bar{I}_2}\mathbf{b}^2 - \frac{1}{3}(\frac{\partial \bar{\Psi}}{\partial \bar{I}_1}\bar{I}_1 + 2\frac{\partial \bar{\Psi}}{\partial \bar{I}_2}\bar{I}_2)\mathbf{1}] \tag{2.7}$$

with $\mathbf{1}$ the tensor identity of second order, $\mathbf{b} = \mathbf{F}\mathbf{F}^T$ left Cauchy-Green tensor and, $\mathbf{F}$ the strain gradient.

2.1.3 Selected hyperelastic model

To determine the parameters of the deformation energy density function, we use the adjustment module provided by Abaqus 6.17 software (numerical modeling that allows you to adjust your test data to a hyperelastic model), which also indicates the range of parameters for which the selected models are stable. The setting was evaluated by several hyperlastic models, as a example, the form of the strain energy potential for some models is presented:

1. Neo-Hookean model

$$\Psi = C_{10}(\bar{I}_1 - 3) + \frac{1}{D_1}(J^{el} - 1)^2 \tag{2.8}$$

where J^{el} is the elastic volume ratio, which relates the total volume ratio, J, and the thermal volume ratio, J^{th}.

2. Polynomial model (N=2)

$$\Psi = \sum_{i+j=1}^{N} C_{ij}(\bar{I}_1 - 3)^i(\bar{I}_2 - 3)^j + \sum_{i=1}^{N} \frac{1}{D_1}(J^{el} - 1)^{2i} \tag{2.9}$$

3. Ogden model

$$\Psi = \sum_{i=1}^{N} \frac{2\mu_i}{\alpha_i}(\lambda_1^{-\alpha_i} + \lambda_2^{-\alpha_i} + \lambda_3^{-\alpha_i} - 3) + \sum_{i=1}^{N} \frac{1}{D_1}(J^{el} - 1)^{2i} \tag{2.10}$$

$\lambda_{1,3}$ are the three invariants of the deformation tensor

Fig.2.3 presents the adjustment and the corresponding coefficients of the experimental data for the tested material with the Ogden N=4 model.

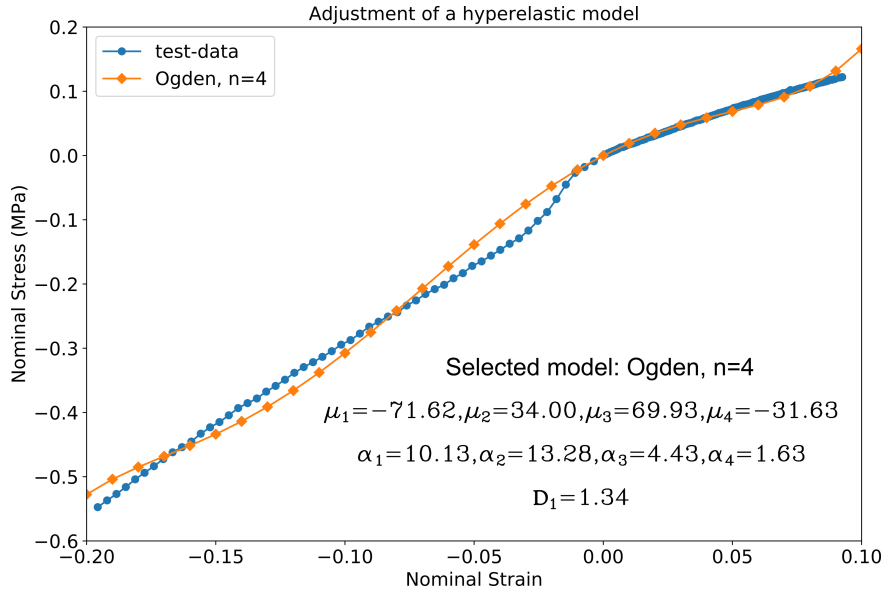

Figure 2.3: Comparative between the proposed hyperelastic model, Ogden N=4 and test data.

2.2 Parametrization of the geometry and factorial design

The geometry of the 1-piece, non-angulated, hydrophobic C-loop IOL was parametrized with six variables (see Fig.2.4): the length ($\lambda_{AA'}$), the width (WH), the thickness (T), and the opening angle (φ) of the haptic, the start of the curvature haptic (HC), and the haptic-optic junction (J). The start of the haptic curvature and the opening angle of the haptic define the overall diameter of the IOL, which ranges from 11.20 to 13.70 *mm*.

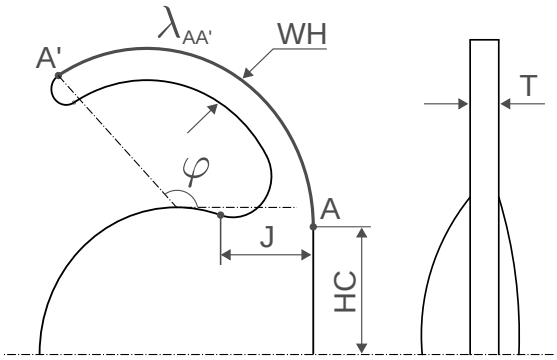

Figure 2.4: Parametrization of the C-loop IOL.

Biomechanical stability was hipothesized to depend on four main parameters: *compression force* –mg– (also referred to as *reaction force*), *axial displacement* –mm–, *tilt* –degrees, °– and *rotation* –degrees, °–. To study the effect of the haptic design on the biomechanical stability, 64 and 144 geometrical variations were created according to the methodology of design of experiments.[40]

First, a 2^k full-factorial design was used to prescreen the most influential geometrical parameters of the IOL and to reduce the number of simulations. A dataset of 64 geometries was built using two levels of variation (Low and High. See Table 2.1) for each of the six parameters under study (i.e., $2^6 = 64$). From the prescreening analysis, the haptic-optic junction (J), the start of the haptic curvature (HC), and the thickness of the haptic (T) were considered as relevant.

Second, a mixed-level full factorial design was used to extend the prior analysis and to gain a deeper insight into the effect of the prescreened relevant variables (i.e., J, HC, T). Importantly, the haptic-optic junction (J) had to be decreased from 1.8 *mm* to 1.2 *mm* for two reasons: first, IOLs became unstable due to the high junction stiffness leading to unrealistic values of axial displacement and tilt; second, its prevalence biased the statistical analysis towards it, making impossible to distinguish

the effect of the remaining design parameters. Hence, only an intermediate level was included for the start of the haptic curvature (HC) and the thickness of the haptic (T), resulting in a mixed-level factorial design of 144 geometries (i.e., $3^2x2^4 = 144$) that combined two parameters at three levels (HC and T), and four parameters at two levels ($\lambda_{AA'}$, WH, φ, J). For the sake of simplicity and to avoid introducing additional bias, the optic was the same for all geometries (+22.00 D), with an appropriate square haptic design. All the parameters were varied according to real measures of available commercial lenses (see Table 2.1).

After generating the dataset of geometrical combinations and associated biomechanical stability, the main effect and interactions of each parameter were studied using analysis of variance (ANOVA). The main effect plots represent the effect of either the individualised mean response for each factor level on the variance of a single outcome. Interaction plots represent how the interaction between two variables affects the variance of a single outcome. Pareto charts were used to represent the degree of influence of each design parameter on the variance of each mechanical stability outcome. Finally, the correlation between design parameters and stability outcomes was studied using the Pearson correlation coefficient (i.e., correlation matrix). All the analysis was performed using Minitab 18 (State College, Pennsylvania, USA) and Python.[41–43] A p-value ≤ 0.05 was considered as statistically significant.

2.3 In silico compression test and determination of mechanical stability

The standardised compression test was performed to approximate the behaviour of the IOL in the capsular bag. Numerical simulations of the mechanical stability

Parameters	**Low Value**	**Middle Value**	**High Value**
$\lambda_{AA'}$: Haptic length (mm)	8.20	–	8.70
WH: Haptic width (mm)	0.40	–	0.65
φ: Opening angle of the haptic (°)	110	–	135
J: Haptic-optic junction (mm)	0.60	–	$\{J_i, J_f\}$
HC: Start of the haptic curvature (mm)	2.00	2.30	2.50
T: Thickness haptic (mm)	0.30	0.35	0.40

Table 2.1: Levels of parameter's variation (Low, Medium and High) involved on the 2^k and mixed-level factorial design. *J_i is the junction for the prescreening analysis ($J_i = 1.8$ mm) while J_f is the junction for the mixed-level factorial design ($J_f = 1.2$ mm).*

of the IOL during a compression test were performed using Abaqus 6.17 (Dassault Systèmes) according to the procedure described in ISO 11979-3. In this compression test, the IOL is placed between two clamps (with a curvature radius of 5 mm) and compressed to measure its mechanical stability. The clamps are initially separated a distance equal to the overall dimension of the IOL to allow its gentle positioning without introducing pretension (see Fig.2.5.a). Then, the right clamp is displaced until a compression diameter of 10 mm while the left clamp remains fixed (see Fig. 2.5.b-c).

The compression (or reaction) force at the horizontal plane was reported only at the end of the compression. The axial displacement, the tilt and the rotation were evaluated by comparing the initial and final configuration of the lens following the Standard ISO 11979-3, which establishes that four key points must be recorded in order to determine the stability of the IOL (see Fig. 2.5.b-c).

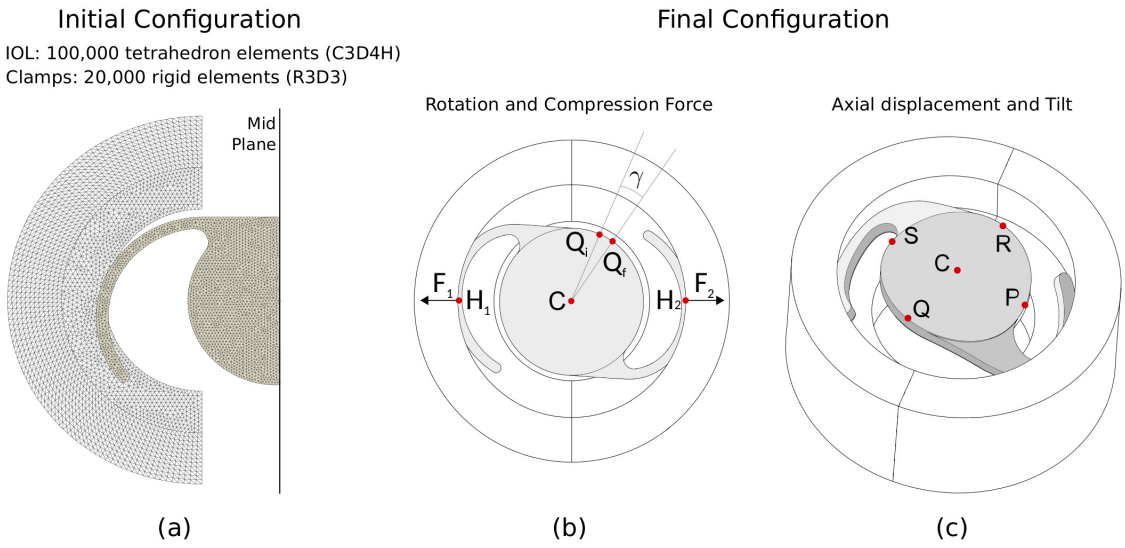

Figure 2.5: In silico model of the compression test. a) Mesh of the in silico model (only half of the model is depicted); b) Measurement of the IOL's rotation and compression (or reaction) force. Rotation is given by the relative angle (γ) between the same point at the beginning (Q_i) and the end (Q_f) of the test. Force is given by the mean of the forces in the haptics ($F = \frac{F_1+F_2}{2}$), with $F_{1,2}$ the absolute value; c) Representation of the key points (in red) used for the evaluation of the tilt (S, R, Q, P) and the axial displacement (C). The tilt was calculated through the next equation, $tilt(^{o}) = \sqrt{s_1^2 + s_2^2}$, with $s_{1,2}$ being the slope between the points S and P, and, Q and R.

Chapter 3

Results

To evaluate the biomechanical stability of the C-Loop IOL, the compression (or reaction) force, the axial displacement, the tilt and the rotation were numerically analysed. After the prescreening analysis (see in Sec.2.2), the haptic-optic junction (J) was recalibrated. High haptic junction values ($\approx$ 1.8 mm) rendered the model unstable leading to unrealistic axial displacements and rotations (see, for example, lens #129 in Table 3.1) which, in turn, resulted in a biased statistical analysis that was insensitive to the perturbation of any other remaining parameter. Accordingly, only results for the mixed-level factorial design (144 IOLs) are presented below. Main effect and interaction plots were analysed to confirm the consistency of the correlation analysis but, since the analysis did not yield any unexpected behaviour, graphical results are not shown here.

Solely based on the Pareto's analysis, the most influential parameters on the mechanical stability seemed to be related to haptic design parameters that control the inertia of the IOL and, therefore, the IOL's bending stiffness.

The compression (or reaction) force is mostly influenced by the width of the haptic (WH – 59.9 %) and the haptic-optic junction (J – 30.5 %) (see Fig.3.a).

The haptic width (WH – 17.7 %) and the start of the haptic curvature (HC – 45.6 %) are the most influential parameters on the axial displacement. Overall, the 75 % of the variance in the axial displacement is mostly explained by the width of the haptic, the haptic-optic junction, the start of the haptic curvature, and the thickness of the haptic (WH, J, HC, T) while the rest of the parameters represent the remaining 25 % of the variance (see in Fig.3.b). Remarkably, the interaction of the haptic width with the haptic-optic junction (WH-J) and the thickness of the haptic (WH-T) represents a non-neligible 15 % of the response, outlining the importance of a careful design of the haptic proportions.

The tilt variance is only affected by the thickness of the haptic (T) and the

LIO Analysed	Factors						Total diameter (mm)	Response			
	$\lambda_{AA'}$	WH	φ	J	HC	T		Compression Force (mg)	Axial displacement (mm)	Tilt (°)	Rotation (°)
#Optimal	8.20	0.40	135	0.60	2.30	0.30	13.25	7.70	0.11	0.09	3.51
#21	8.20	0.40	135	1.80	2.30	0.40	13.25	302.11	0.21	0.10	4.95
#27	8.20	0.40	135	1.20	2.30	0.40	13.25	33.34	0.13	0.01	4.06
#35	8.20	0.40	110	0.60	2.30	0.35	13.50	13.87	0.15	0.05	4.24
#52	8.20	0.40	110	0.60	2.50	0.40	13.90	18.89	0.13	0.03	4.62
#87	8.80	0.40	135	0.60	2.30	0.35	13.25	12.57	0.12	0.05	2.96
#129	8.20	0.65	135	1.80	2.30	0.40	13.25	328.32	0.96	0.18	4.89
#139	8.80	0.65	135	0.60	2.30	0.30	13.25	36.60	0.19	0.04	4.86

Table 3.1: Individualised results for representative IOLs. Design parameters are: the length ($\lambda_{AA'}$), width (WH) and opening angle of the haptic (φ), the haptic-optic junction (J), start of the haptic curvature (HC) and the thickness (T).

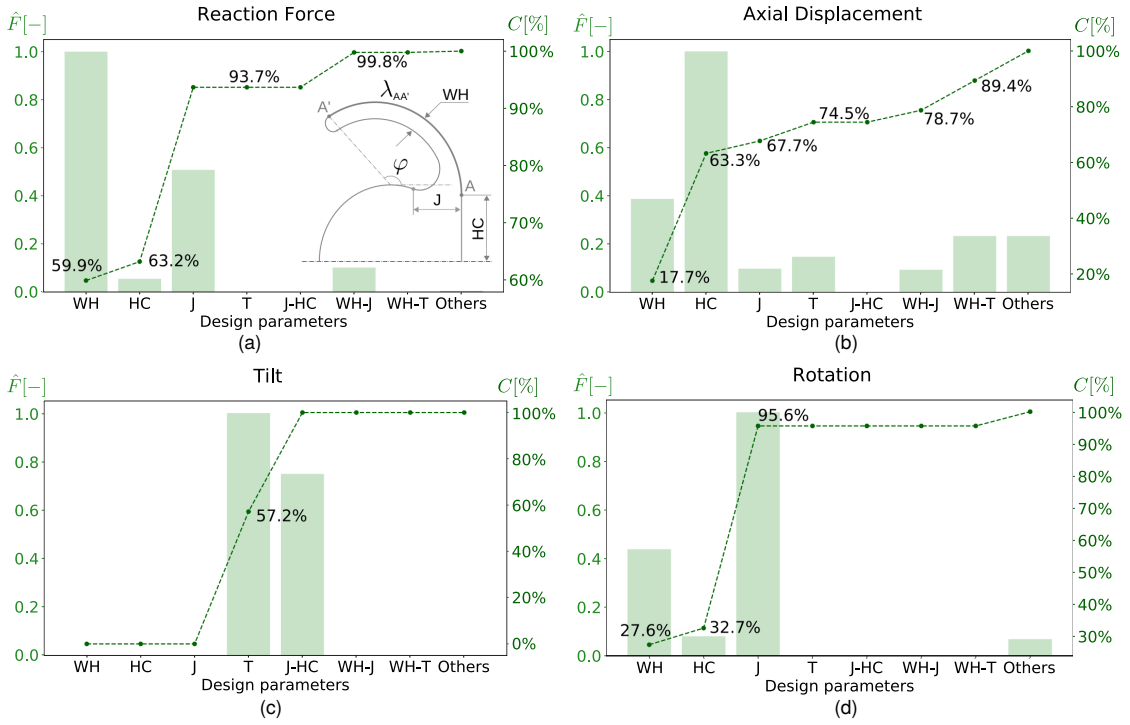

Figure 3.1: Pareto charts for the mixed-level ($3^2x2^4 = 144$) factorial design for different responses. Only statistically significant terms are depicted. Parameters with a contribution of less than a 5 % were grouped in others. $\hat{F}$ is the normalized F-stat and $C[\%]$ is the percentage of contribution. a) Compression (or reaction) force; b) Axial displacement; c) Tilt; d) Rotation; *Legend*: the factors and interactions shown are: the length of the haptic ($\lambda_{AA'}$), the width of the haptic (HW), the opening angle of the haptic (φ), the start of the haptic curvature (HC), the haptic-optic junction (J), and the thickness of the haptic (T).

interaction between the haptic-optic junction and the start of the haptic curvature (J-HC) (see Fig.3.c).

The variance in the rotation of the IOL is mainly explained by the start of the haptic curvature (HC – 62.9 %) and the width of the haptic (WH – 27.6 %) (see Fig.3.d).

Further analysis based on the Pearson correlation matrix (see Fig.3.2) supported these findings.

The compression (or reaction) force was confirmed to be strongly and directly correlated with the haptic width (WH), the haptic-optic junction (J) and the start of the haptic curvature (HC). This direct correlation would result in a moderate (J and HC) to strong (WH) increment in the reaction force if these parameters are increased. Also, a low inverse correlation was found with the haptic angle (φ), likely resulting in a low reduction in force if the angle is increased.

The axial displacement presented moderate to low direct correlations with the haptic width (WH), the haptic-optic juncion (J) and the start of the haptic curvature (HC), and moderate to low inverse correlations to the haptic thickness (T) and the haptic angle (φ). These correlations would suggest to decrease WH, J, or HC, or to decrease T and φ in order to reduce the axial displacement.

The tilt presents a low inverse correlation to the haptic length ($\lambda_{AA'}$) and the thickness of the haptic (T), and a low direct correlation to the haptic width (WH) and the start of the haptic curvature (HC). These correlations suggest a difficult control of the IOL's tilt just using the proposed design parameters.

The rotation of the lens presents a strong direct correlation to the start of the haptic curvature (HC), a moderate direct correlation to the haptic width (WH), and a low inverse correlation to the haptic length ($\lambda_{AA'}$) and the haptic-optic junction (J). These correlations would suggest to reduce HC and WH, or to increase $\lambda_{AA'}$ and J to obtain a lower rotation of the lens.

Finally, the compression (or reaction) force, the axial displacement and the rotation of the C-loop IOL present a moderate direct correlation between them, while the tilt loosely correlated to the other stability parameters.

Individualised biomechanical responses for representative IOLs are presented in Table 3.1. Again, tilt does not seem to be highly influenced by any design parameter in particular, almost resulting in a design-independent factor with a maximum variation up to 1°. The Fig.3.3 represents the IOLs shown in Table 3.1 to appreciate the values in the different design parameters.

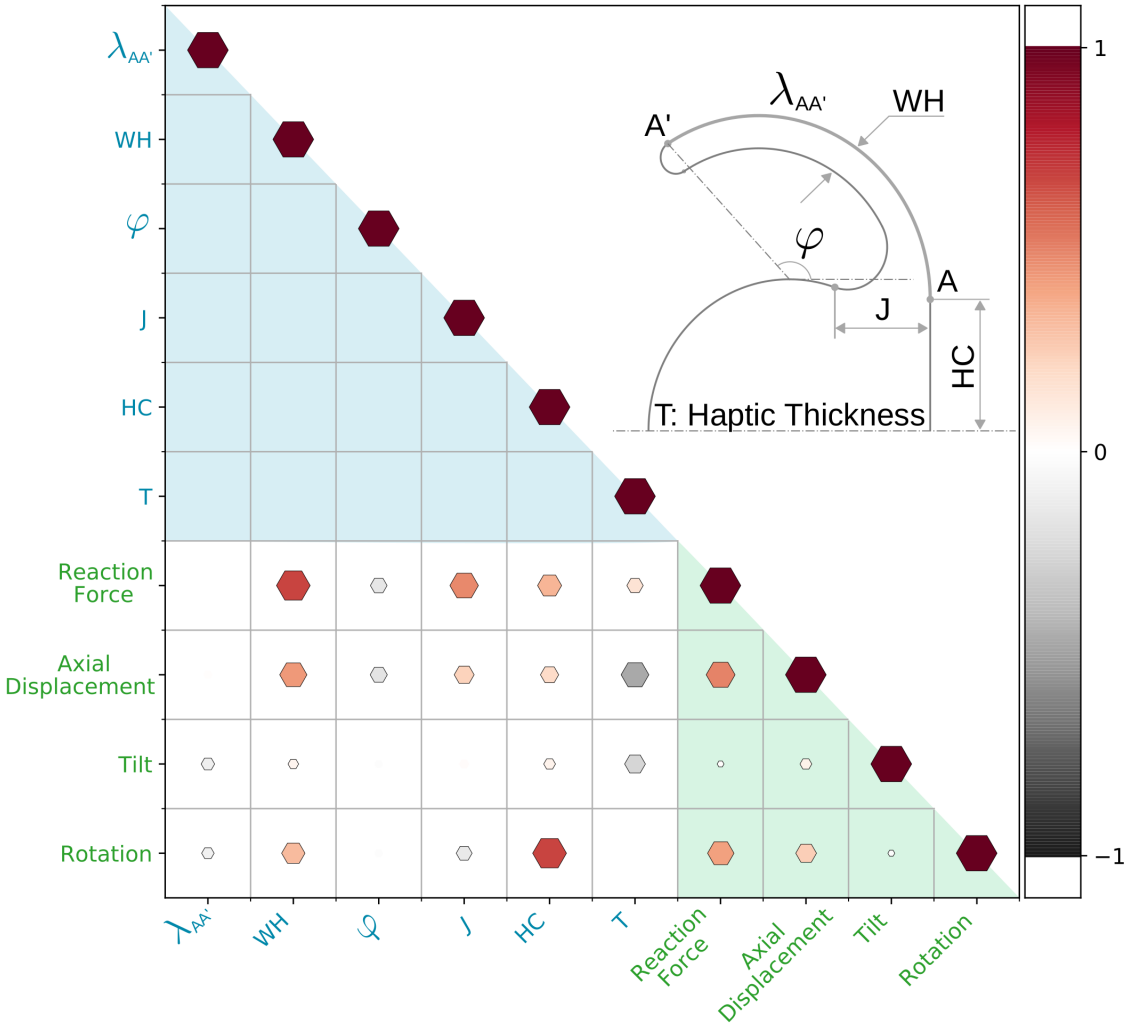

Figure 3.2: Pearson correlation matrix (mixed-level factorial design, $3^2x2^4 = 144$). Design parameters (in blue): the length ($\lambda_{AA'}$), width (WH), thickness (T) and opening angle of the haptic (φ), the haptic-optic junction (J), and the start of the haptic curvature (HC) and the thickness (T). Biomechanical stability outcomes (in green): rotation, compression (or reaction) force, axial displacement and tilt. Size of the hexagons depicts the degree of linear correlation: the bigger the size, the greater the linear correlation. Color of the hexagons depicts whether the linear correlation is direct (positive) or inverse (negative) (reddish palette – direct; grayish palette – inverse).

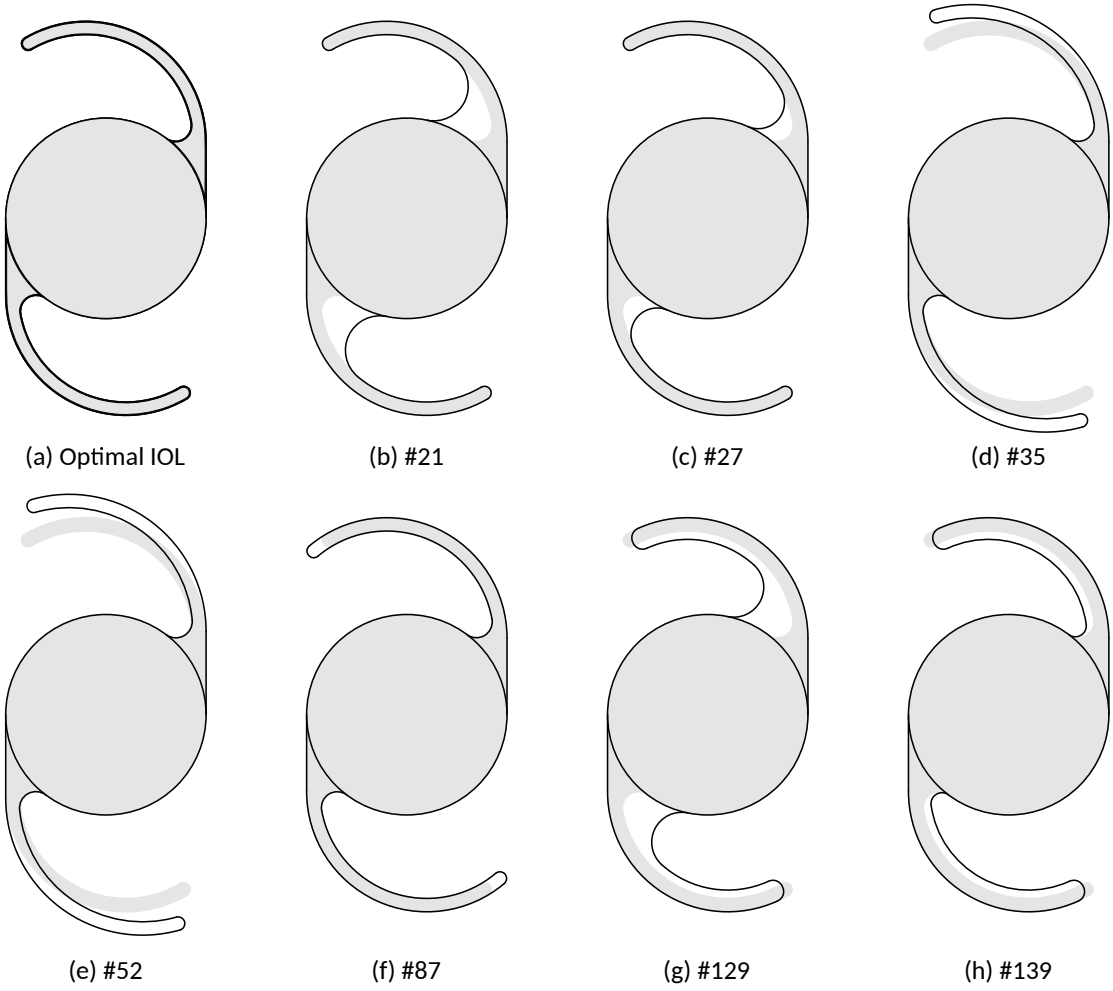

Figure 3.3: Geometric design of IOLs analysed in the Table 3.1. The optimal geometry (a) is superposed in gray upon the different select geometrical variations.

Chapter 4

Conclusions and Future Lines

This chapter firstly exposes a discussion of the results obtained, then the main conclusions obtained and finally, the future lines of research proposed as a continuation of this Final Master's Thesis.

4.1 Discussion

Postoperative IOL stability is determinant for the adequate performance of premium IOLs. Decentration, tilt, rotation or axial displacement can severely affect the postsurgical visual acuity of the patient.[5,44] Although several studies have evaluated these stability parameters after implantation in a pseudophakic eye,[29,30] it is still not possible to predict the postoperative performance and the mechanical behaviour before cataract refractive surgery.

In the present work, we have introduced the first systematic study that analyses the biomechanical stability of 1-piece, non-angulated, hydrophobic C-loop IOLs with respect to different design factors. To save costs in experiments, a previous in silico platform[25] has been used to simulate the mechanical compression test described in the Standard ISO 11972-3.[31] This test is the companies' gold standard for testing the mechanical stability of commercial lenses. The in silico platform allowed for testing 144 geometrical variations that were known to behave mechanically sound. The use of in silico models along with advanced statistical tools (i.e., mixed-level factorial analysis) allowed for studying the impact of design factors (length, width, thickness and opening angle of the haptic, the start of the haptic curvature, and the haptic-optic juction) on the biomechanical stability of the lens (compression force –mg–, axial displacement –mm–, tilt –degrees, °– and rotation –degrees, °–). Although only a 1-piece hydrophobic IOL with non-angulated C-loop haptics and

a dioptric power (+22.00D) was considered, the proposed methodology allows for a straightforward implementation of different IOL features such as the style of the plate haptic, multipiece IOLs, different dioptric powers, or different capsular bags.

Based on the present results, the width (WH) and thickness (T) of the haptic, the start of the haptic curvature (HC), and the haptic-optic junction (J) are suggested to be important factors determining the biomechanical stability of the lens. When the cross-section of the haptic increases (i.e., increased haptic width and/or thickness) and the haptic-optic junction is larger, the energy accumulated by the IOL is higher and will result on higher rotations, axial displacements and reaction forces (see, for example, IOLs #21 and #129 in Table 3.1 or in Fig.4.1). Therefore, a delicate trade-off between the length ($\lambda_{AA'}$) and the cross-section of the haptic must be achieved to minimize undesired postsurgical shifts.

Individually, different stability outcomes are influenced by different design parameters: the compression (or reaction) force by the width of the haptic (WH), the haptic curvature start (HC) and the haptic-optic union (J); the axial displacement by the width (WH) and thickness (T) of the haptic, and the haptic-optic union (HC); the tilt by the thickness of the haptic (T); and the rotation by the haptic width (WH) and the haptic curvature start (HC).

In particular, the trend in the results suggests that the haptic-optic junction (J), the start of the haptic curvature (HC) and the haptic width (WH) are the most influential factors for all responses except for the tilt. Reducing the haptic-optic junction (J – 0.6 mm) and the haptic width (WH – 0.40 mm) lead to designs with better biomechanical stability.

In this vein, Lane et al.[27] compared the mechanical characteristics and stability of 5 currently marketed monofocal IOLs finding that designs with flexible hinges, as the present in the Clareon CNA0T0 or AcrySof SN60WF (Alcon Laboratories, Inc.), improved the axial stability. This finding aligns well with our results in which the more flexible the haptic-optic junction, the better is the stability in terms of compression force and axial displacement. On the other hand, the least influential factor on the biomechanical stability is the haptic length ($\lambda_{AA'}$), as it had a low effect in the rotation, axial displacement or reaction force.

Unfortunately, in order to minimize the rotation of the lens, the optimal configuration would require of a larger haptic-optic juntion (J) which is incompatible with minimizing, for example, the axial displacement. In the same vein, reducing the haptic thickness (T) would lead to an increased tilt and axial displacement, but a lower compression force. Due to this inverse coupling between design parameters, different design strategies are mandatory depending on the stability factor that is aimed at being minimized.

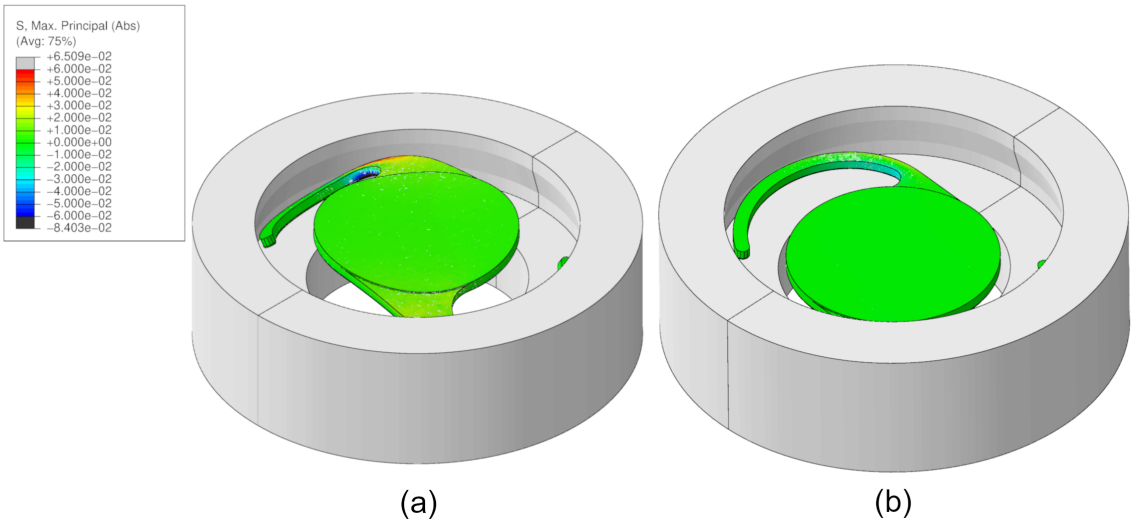

Figure 4.1: Maximum principal stresses at $10mm$ closure. a) #129 IOL. b) #21, the optimal IOL. In addition to obtaining a correct positioning, the optic of the IOL does not suffer any stress. Thus, the patient's visual quality would be adequate.

If the compresion (or reaction) force, the axial displacement and the tilt aim at being minimised, then IOLs should tend to reduce their haptic width (WH) and the start of the haptic curvature (HC), while increasing the opening angle (φ) and the haptic thickness (T). Providing that this design restriction is complied with, the diameter of the lens should not affect and could be individually designed to fit in the capsular bag of each patient.

Remarkably, our in silico platform behaved within the experimental reported ranges and complied with the current manufacturing norms. Lane et al.[26] reported that the multipiece AcrySof MA30BA IOL (Alcon Laboratories, Inc.) presented the greatest axial displacement when compared to four single-piece IOLs (1.98 mm versus 0.15 $\pm$ 0.40 mm, respectively). Later on, same authors reported that, under dynamic compression up to 10 mm, the range of axial displacement varied from -0.01 mm (model AcrySof SN60WF, Alcon Laboratories, Inc.) to 0.68 mm (model MX60, Bausch C Lomb, Inc.). Bozukava et al.[32] reported a range of axial displacement from 0.00 mm to 1.032 mm when the IOLs were compressed up to 10.0 mm. Similar range of axial displacement (0.11 to 0.96 mm) was obtained for #129 IOL variations in the present study (see extract in Table 3.1).

The International Standards ISO 11979-2:2014[45] specifies that, for manufacturing toric IOLs, the angle difference between the physical axis indicator and the meridian with the lowest dioptic power must be less and equal than 5°. In the present study, the range of rotation varied from 2.96° to 4.95°, being 3.51° the value for the optimal design (see extract in Table 3.1).

To the best of our knowledge, we presented the first in silico platform amenable for determining a set of optimum design parameters for 1-piece, non-angulated, hydrophobic C-Loop IOLs, see final deformation in Fig.4.1. For the first time, a numerical platform allowed to systematically estimate the biomechanical stability of different geometrical variations, scientifically supporting the intuition that more slender haptics would lead to a better biomechanical stability. Not only that, but our optimal in silico design is quite close to current commercial designs with the best clinical performance (AcrySof SN60WF and Tecnis ZCB00).

4.2 Conclusions

From the discussion commented above, the main conclusions of this TFM are:

- The haptic-optic junction is the main design parameter of the C-loop IOLs.
- The width and the start of the curvature haptic highly influence on a adequate response of the IOL.
- A method for determing a set of optimum C-loop IOL designs is achieved. Resulting in a custom design.

4.3 Future Lines

The future use of these in silico models along with clinical data can be used to increase the predictability of the stability of the IOLs in the capsular bag after a cataract refractive surgery. This will lead to reduced costs by exploring a feasible space of solutions during the product design process and before manufacturing. In sum, this methodology represents a first step towards the customization of IOLs (i.e., choosing the optimal size of the IOL depending on the eyeball's axial length of a patient, or the diameter of the capsular bag). Therefore, our next study will be focused on simulating the emplacement of an IOL inside the capsular bag, see Fig.4.2. In order to analyse the effect on the patient's visual acuity, the following lines will be studied:

- The size of the capsular bag.
- The capsular material behaviour.
- The emplacement of the IOL in the cataract surgery.
- The position of the lens in the accommodative process of the eye.

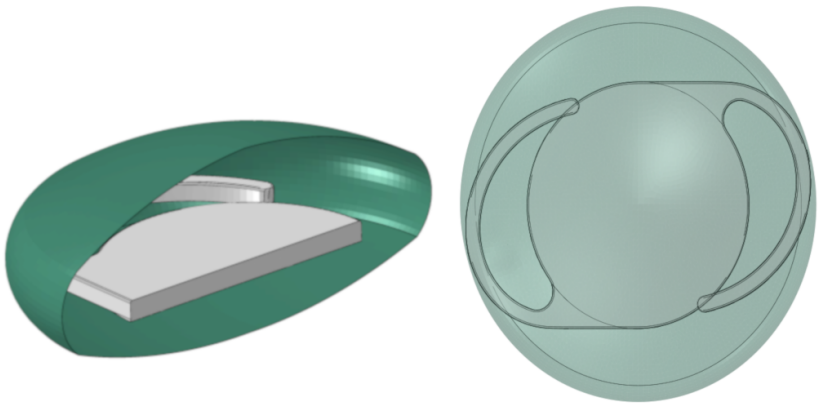

Figure 4.2: Simulation of an intraocular lens inside the capsular bag. a) Isometric view with a cut on the y-axis. b) Plan view

Bibliography

[1] Garzón N, Poyales F, Ortíz B, Ruiz-García JL, Quiroga JA. Evaluation of Rotation and Visual Outcomes After Implantation of Monofocal and Multifocal Toric Intraocular Lenses. *J Refract Surg.* 2015;31:90–97.

[2] Alió JL, Plaza-Puche AB, Javaloy J, Ayala MJ, Vega-Estrada A. Clinical and Optical Intraocular Performance of Rotationally Asymmetric Multifocal IOL Plate-Haptic Design Versus C-Loop Haptic Design. *J Refract Surg.* 2013;29:252–259.

[3] Pérez-Merino P, Marcos S. Effect of intraocular lens decentration on image quality tested in a custom model eye. *J Cataract Refract Surg.* 2018;44:889–896.

[4] Alio JL, Plaza-Puche AB, Férnandez-Buenaga R, Pikkel J, Maldonado M. Multifocal intraocular lenses: An overview. *Surv Ophthalmol.* 2017;62:611–634.

[5] Woodward MA, Randleman JB, Stulting R Doyle. Dissatisfaction after multifocal intraocular lens implantation. *J Cataract Refract Surg.* 2009;35:992–997.

[6] Linnola RJ, Sund M, Ylönen R, Pihlajaniemi T. Adhesion of soluble fibronectin, laminin, and collagen type IV to intraocular lens materials. *J Cataract Refract Surg.* 1999;25:1486–1491.

[7] Lombardo M, Carbone G, Lombardo G, De-Santo MP, Barberi R. Alysis of intraocular lens surface adhesiveness by atomic force microscopy. *J Cataract Refract Surg.* 2009;35:1266–1272.

[8] Crnej A, Hirnschall N, Nishi Y, et al. Impact of intraocular lens haptic design and orientation on decentration and tilt. *J Cataract Refract Surg.* 2011;37:1768–1774.

[9] Choi M, Lazo MZ, Kang M, Lee J, Joo CK. Effect of number and position of intraocular lens haptics on anterior capsule contraction: a randomized, prospective trial. *BMC Ophthalmol.* 2018;18.

[10] Chang DF. Early rotational stability of the longer Staar toric intraocular lens. *J Cataract Refract Surg.* 2003;29:935–940.

[11] Shah GD, Praveen MR, Vasavada AR, Vasavada VA, Rampal G, Shastry LR. Rotational stability of a toric intraocular lens: Influence of axial length and alignment in the capsular bag. *J Cataract Refract Surg.* 2012;38:54–59.

[12] Nagy ZZ, Kránitz K, Takacs AI, Miháltz K, Kovács I, Knorz MC. Comparison of Intraocular Lens Decentration Parameters After Femtosecond and Manual Capsulotomies. *J Refract Surg.* 2011;27:564–569.

[13] Ridley Harold. Intra-ocular acrylic lenses after cataract extraction. *The Lancet.* 1952;259:118–121.

[14] Werner L. Biocompatibility of intraocular lens materials. *Curr Opin Ophthalmol.* 2008;19:41–49.

[15] Vounotrypidis E, Lackerbauer C, Kook D, Dirisamer M, Priglinger S, Mayer W. Influence of total intraocular lens diameter on efficacy and safety for in the bag cataract surgery. *Oman J Ophthalmol.* 2018.

[16] Werner L, Tetz M, Feldmann I, Bücker M. Evaluating and defining the sharpness of intraocular lenses: Microedge structure of commercially available square-edged hydrophilic intraocular lenses. *J Cataract Refract Surg.* 2009;35:556–566.

[17] Wirtitsch MG, Findl O, Menapace R, et al. Effect of haptic design on change in axial lens position after cataract surgery. *J Cataract Refract Surg.* 2004;30:45–51.

[18] Miháltz K, Lasta M, Burgmüller M, Vécsei-Marlovits PV, Weingessel B. Comparison of Two Toric IOLs with Different Haptic Design: Optical Quality after 1 Year. *J Ophthalmol.* 2018;2018:1–7.

[19] Bozukova D, Werner L, Mamalis N, et al. Double-C loop platform in combination with hydrophobic and hydrophilic acrylic intraocular lens materials. *J Cataract Refract Surg.* 2015;41:1490–1502.

[20] Chang DF. Comparative rotational stability of single-piece open-loop acrylic and plate-haptic silicone toric intraocular lenses. *J Cataract Refract Surg.* 2008;34:1842–1847.

[21] Patel CK, Ormonde S, Rosen PH, Bron AJ. Postoperative intraocular lens rotation. *Ophthalmology.* 1999;106:2190–2196.

[22] Prinz A, Neumayer T, Buehl W, et al. Rotational stability and posterior capsule opacification of a plate-haptic and an open-loop-haptic intraocular lens. *J Cataract Refract Surg.* 2011;37:251–257.

[23] Chua WH, Yuen LH, Chua J, Teh G, Hill WE. Matched comparison of rotational stability of 1-piece acrylic and plate-haptic silicone toric intraocular lenses in Asian eyes. *J Cataract Refract Surg.* 2012;38:620–624.

[24] Petternel V, Menapace R, Findl O, et al. Effect of optic edge design and haptic angulation on postoperative intraocular lens position change. *J Cataract Refract Surg.* 2004;30:52–57.

[25] Remón L, Siedlecki D, Cabeza-Gil I, Calvo B. Influence of material and haptic design on the mechanical stability of intraocular lenses by means of finite-element modeling. *J Biomed Opt.* 2018;23:1.

[26] Lane SS, Burgi P, Milios GS, Orchowski MW, Vaughan M, Schwarte E. Comparison of the biomechanical behavior of foldable intraocular lenses. *J Cataract Refract Surg.* 2004;30:2397–2402.

[27] Lane S, Collins S, Das KK, et al. Evaluation of intraocular lens stability. *J Cataract Refract Surg.* 2018.

[28] Hayashi K, Hayashi H. Comparison of the stability of 1-piece and 3-piece acrylic intraocular lenses in the lens capsule. *J Cataract Refract Surg.* 2005;31:337–342.

[29] Kumar DA, Amar A, Prakash G, Jacob S, Saravanan Y, Agarwal A. Evaluation of Intraocular Lens Tilt With Anterior Segment Optical Coherence Tomography. *Am J Ophthalmol.* 2011;151:406–412.e2.

[30] Poyales F, Garzón N, Pizarro D, Cobreces S, Hernández A. Stability and visual outcomes yielded by three intraocular trifocal lenses with same optical zone design but differing material or toricity. *Eur J Ophthalmol.* 2018:112067211879506.

[31] *BS EN ISO 11979-3:2012 Ophthalmic implants. Intraocular lenses. Mechanical properties and test methods.* BSI Standards Limited 2012.

[32] Bozukova D, Pagnoulle C, Jérôme C. Biomechanical and optical properties of 2 new hydrophobic platforms for intraocular lenses. *J Cataract Refract Surg.* 2013;39:1404–1414.

[33] Draschl P, Hirnschall N, Luft N, et al. Rotational stability of 2 intraocular lenses with an identical design and different materials. *J Cataract Refract Surg.* 2017;43:234–238.

[34] Flaxman Seth R, Bourne Rupert R A, Resnikoff Serge, et al. Global causes of blindness and distance vision impairment 1990–2020: a systematic review and meta-analysis *The Lancet Global Health.* 2017;5:e1221–e1234.

[35] Development Benz Research &. Intraocular Lens Materials & Manufacturing Technology 2013.

[36] *UNE-ISO 7743:2016. Elastómeros, vulcanizados o termoplásticos. Determinación de las propiedades esfuerzo/deformación en compresión.* . 2016.

[37] *UNE-ISO 37:2013. Elastómeros. Caucho, vulcanizados o termoplásticos. Determinación de las propiedades de esfuerzo-deformación en tracción.* . 2013.

[38] Simo J. C., Taylor R. L., Pister K. S. Variational and Projection Methods for the Volume Constraint in Finite Deformation Elasto-Plasticity. *Computer Methods in Applied Mechanics and Engineering.* 1985;51:177-208.

[39] Simo J. C., Taylor R. L., Pister K. S.. Variational and Projection Methods for the Volume Constraint in Finite Deformation Elasto-Plasticity *Computer Methods in Applied Mechanics and Engineering.* 1985;51:177-208.

[40] Montgomery D. *Design & Analysis of Experiments. 5ed.* New York: John Wiley 2001.

[41] V Rossum Guido, Drake FL. *Python 3 Reference Manual.* Paramount, CA: CreateSpace 2009.

[42] Oliphant Travis E. *A guide to NumPy*;1. Trelgol Publishing USA 2006.

[43] Hunter J. D.. Matplotlib: A 2D Graphics Environment *Computing in Science Engineering.* 2007;9:90-95.

[44] Zvorničanin J, Zvorničanin E. Premium intraocular lenses: The past, present and future. *J Curr Ophthalmol.* 2018;30:287–296.

[45] *BS EN ISO 11979-2:2014 Ophthalmic implants - Intraocular lenses. Part 2: Optical properties and test methods.* BSI Standards Limited 2014.